MATHEMATICAL MODELING OF THE FLOW FIELD AND PARTICLE MOTION IN A ROTATING BIOREACTOR AT UNIT GRAVITY AND MICROGRAVITY

Final Report

NASA/ASEE Summer Faculty Fellowship Program 1990

Johnson Space Center

Prepared by:	Ernest J. Boyd, Ph.D.
Academic Rank:	Associate Professor
University & Department:	Mankato State University Department of Mathematics, Astronomy & Statistics Mankato, Minnesota 56002-8400
NASA/JSC	
Directorate:	Space and Life Sciences
Division:	Medical Sciences
Branch:	Biomedical Operations & Research
JSC Colleague:	Steve Gonda, Ph.D.
Date Submitted:	August 23, 1990
Contract Number:	NGT-44-005-803

ABSTRACT

The biotechnology group at NASA Johnson Space Center is developing systems for culturing mammalian cells that simulate some aspects of microgravity and provide a low shear environment for microgravity-based studies on suspension and anchorage-dependent cells. The design of these vessels for culturing cells is based on the need to suspend cells and aggregates of cells and microcarrier beads continually in the culturing medium. The design must also provide sufficient circulation for adequate mass transfer of nutrients to the cells and minimize the total force on the cells. Forces, resulting from sources such as hydrodynamic fluid shear and collisions of cells and walls of the vessels, may damage delicate cells and degrade the formation of three-dimensional structures. This study examines one particular design in both unit gravity and microgravity based on two concentric cylinders rotating in the same direction at different speeds to create a Couette flow between them. The study presents a numerical simulation for the flow field and the trajectories of particles in the vessel. The flow field for the circulation of the culturing medium is modelled by the Navier-Stokes equations. The forces on a particle are assumed to be drag from the fluid's circulation, buoyancy from the gravitational force and centrifugal force from the rotation of the vessel. The problem requires first solving the system of partial differential equations for the fluid flow by a finite difference method and then solving the system of ordinary differential equations for the trajectories by Gear's stiff method. Results of the study indicate that the trajectories in unit gravity and microgravity are very similar except for small spatial deviations on the fast time scale in unit gravity. The total force per unit cross-sectional area on a particle in microgravity, however, is significantly smaller than the corresponding value in unit gravity, which is also smaller than anticipated. Hence, this study indicates that this design for a bioreactor with optimal rates of rotation can provide a good environment for culturing cells in microgravity with adequate circulation and minimal force on the cells.

The biotechnology group at NASA Johnson Space Center is developing rotating cylindrical bioreactors for culturing anchorage-dependent mammalian cells on microcarrier beads. The design of the vessels is motivated by the need to keep the aggregates of cells and microcarriers suspended in the culturing medium, to provide sufficient circulation for adequate mass transfer of nutrients to the cells and to minimize the forces on the cells. These forces, resulting from sources such as hydrodynamic fluid shear and collisions of cells and walls of the vessels, may damage delicate cells and degrade the formation of three-dimensional structures. Several studies, such as the research reported by Cherry and Papoutsakis (refs. 1 and 2) and by Croughan, Hamel and Wang (refs. 3 and 4), have examined ways to quantitate the hydrodynamic effects damaging the cells. However, these reports do not consider the complete dynamics of a particle's motion relative to the fluid. The purposes of this study are to develop a mathematical simulation of a particle's motion and to calculate the total force on a particle suspended in a rotating cylindrical bioreactor.

To begin this study a simple geometry for the vessel was chosen in order to provide a uniform flow field throughout the vessel. The vessel consists of two concentric cylinders both 11 cm long with the outer cylinder having a radius of $r_o = 4.0$ cm and rotating at ω_o rpm's, while the inner cylinder has a radius of $r_i = 2.86$ cm and rotating in the same direction at ω_i rpm's. This narrow gap of 1.14 cm between the cylinders is completely filled with culturing medium into which particles as aggregates of cells and microcarrier beads are introduced. Figure 1 provides a schematic representation of the vessel. Cylindrical coordinates (r, θ, z) will be used to indicate positions within the vessel where r is the radial component outward relative to the cylinders with $r_i \leq r \leq r_o$, θ is the angular component measured positively in the direction of rotation of the two cylinders, and z is the axial direction oriented horizontally in a gravitational field with $0 \leq z \leq 11$. Mathematical simulations of more complex geometries, including perfusion of culturing medium, are being planned.

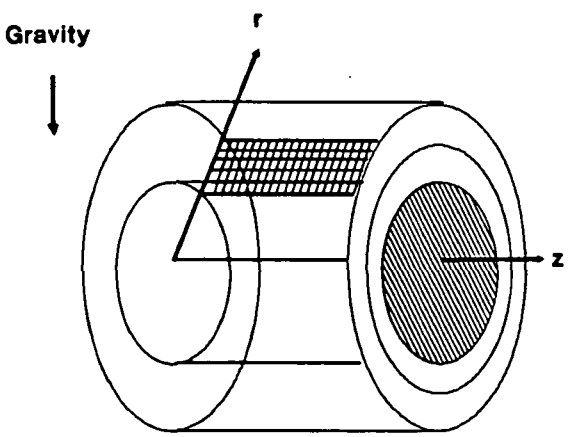

Figure 1.- Schematic representation of the rotating bioreactor.

Assumptions for this mathematical simulation are:

1. The culturing medium is a Newtonian fluid with constant density ρ_s measured in gr/cm^3 and constant viscosity μ measured in gr/cm sec;

2. Particles are spherical in shape with diameter d measured in cm and density ρ_p measured in gr/cm^3, do not interact with one another, and do not affect the flow of the culturing medium;
3. The flow of the culturing medium caused by the rotation of the concentric cylinders is a laminar, axially symmetric Couette flow and is modeled by the Navier-Stokes equations; and
4. The forces acting on a particle are drag from the fluid's circulation, buoyancy from the gravitational force relative to the difference between the densities of a particle and the fluid, and centrifugal force from the rotation of the vessel.

If (u, v, w) represent the (radial, circumferential, axial) components of the velocity of the flow field measured in cm/sec, then the equations for the flow field are:

(1) $$\frac{1}{r}\frac{\partial(ru)}{\partial r} + \frac{\partial w}{\partial z} = 0$$

(2) $$\frac{Du}{Dt} - \frac{v^2}{r} = \frac{\mu}{\rho_s}\left(\nabla^2 u - \frac{u}{r^2}\right)$$

(3) $$\frac{Dv}{Dt} - \frac{uv}{r} = \frac{\mu}{\rho_s}\left(\nabla^2 v - \frac{v}{r^2}\right)$$

and

(4) $$\frac{Dw}{Dt} = -\frac{1}{\rho_s}\frac{\partial P}{\partial z} + \frac{\mu}{\rho_s}\nabla^2 w$$

where

$$\frac{D}{Dt} = \frac{\partial}{\partial t} + u\frac{\partial}{\partial r} + w\frac{\partial}{\partial z}$$

$$\nabla^2 = \frac{1}{r}\frac{\partial}{\partial r}\left(r\frac{\partial}{\partial r}\right) + \frac{\partial^2}{\partial z^2}$$

and P is the fluid pressure measured in gr/cm sec^2. Note that axial symmetry implies that all derivatives with respect to θ in the Navier-Stokes equations are zero. Boundary conditions for the flow field are the standard constraints of no slip and no penetration.

The equations for a trajectory of a particle are:

(5) $$m\frac{d^2 r}{dt^2} = -\alpha\left(\frac{dr}{dt} - u\right) - \beta g\cos\theta + \beta r\left(\frac{d\theta}{dt}\right)^2$$

(6) $$mr\frac{d^2\theta}{dt^2} = -\alpha\left(r\frac{d\theta}{dt} - v\right) - \beta g\sin\theta$$

and

(7) $$m\frac{d^2z}{dt^2} = -\alpha\left(\frac{dz}{dt} - w\right)$$

where $m = \rho_p \pi d^3/6$, $\alpha = 3\pi d\mu$, $\beta = (\rho_p - \rho_s)\pi d^3/6$ and g is the acceleration due to gravity measured in cm/sec^2. In this study initial conditions for a particle at $t = 0$ are $r = 3$, $\theta = 0$, $z = 1, 2.5, 4, 7, 8.5$ or 10, and the derivatives are all zero.

The values of the parameters for this study are $d = 0.0175$ cm, $\rho_s = 1.02$ gr/cm^3, $\rho_p = 1.04$ gr/cm^3, and $\mu = 0.0097$ gr/cm sec. These values are approximately correct for the type of medium and microcarrier beads being used by the biotechnology group at NASA Johnson Space Center. Preliminary studies consist of four trials using different rotating speeds ω_i and ω_o for the inner and outer cylinders. The speeds are listed in Table 1 below. These values provide numerical results from which optimal rotating speeds hopefully may be estimated.

TABLE 1.- SPEED OF ROTATION IN RPM'S.

Trial	Inner Cylinder, ω_i	Outer Cylinder, ω_o	Differential Rate
1	24	18	6
2	30	18	12
3	36	18	18
4	36	12	24

Dr. Yowmin David Tsao at NASA Johnson Space Center used a semi-implicit finite difference algorithm employing a hybrid scheme developed by Spalding (ref. 5) to compute the values of (u, v, w) from the system of partial differential equations in Equations 1 - 4 on a discrete grid. The grid has 61 subdivisions in the z-direction and ten subdivisions in the r-direction. Since the flow field is axially symmetric, it can be projected into this rectangular region of the (z, r)-plane. Note that v is closely approximated by the standard formula for Couette flow (ref. 6):

(8) $$v = \frac{1}{r_o^2 - r_i^2}\left[r\left(\omega_o r_o^2 - \omega_i r_i^2\right) - \frac{r_o^2 r_i^2}{r}(\omega_o - \omega_i)\right]$$

with ω_i and ω_o measured in radians. The finite difference program was advanced in time t until a steady-state flow was assumed to be reached. This data for the numerical values of the flow field on the rectangular grid was provided to the author, who used linear interpolation to produce an approximation to the complete, steady-state, axially symmetric flow field for (u, v, w) as functions of (r, z).

Figures 2 - 5 show segments of the secondary flow fields for the four trials. Printed along each streamline is the circulation time in seconds computed for the segment plotted in the (z, r)-plane. Circulation is a two-compartmental flow with counterclockwise circulation in the left half and clockwise circulation in the right half. A Runge-Kutta-Fehlberg numerical method (ref. 7) was used to generate the streamlines by solving $dr/dt = u(r, z)$ and $dz/dt = w(r, z)$. However, the zero boundary conditions along the walls of the vessel and the limitations in numerical accuracy due to the linear interpolation of the data for the flow field prevent the complete circulation from being plotted along streamlines in the neighborhoods of the end walls of the vessel. In these narrow regions circulation will be

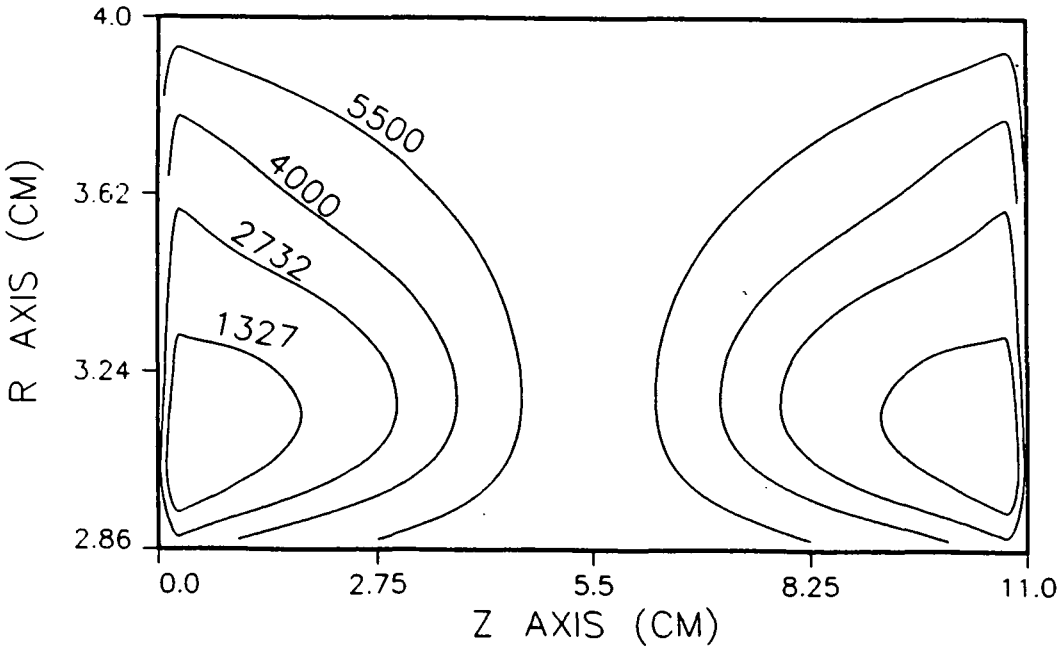

Figure 2.- Streamlines in the *zr* - plane for Trial 1
with the outer cylinder rotating at 18 rpm and the inner cylinder rotating at 24 rpm.

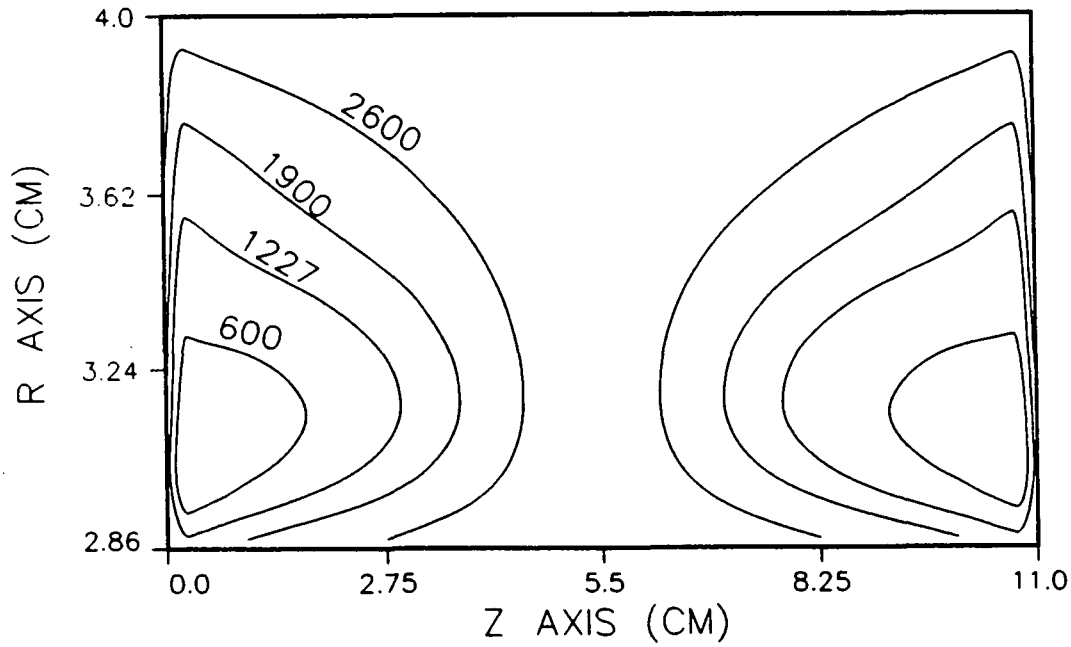

Figure 3.- Streamlines in the *zr* - plane for Trial 2
with the outer cylinder rotating at 18 rpm and the inner cylinder rotating at 30 rpm.

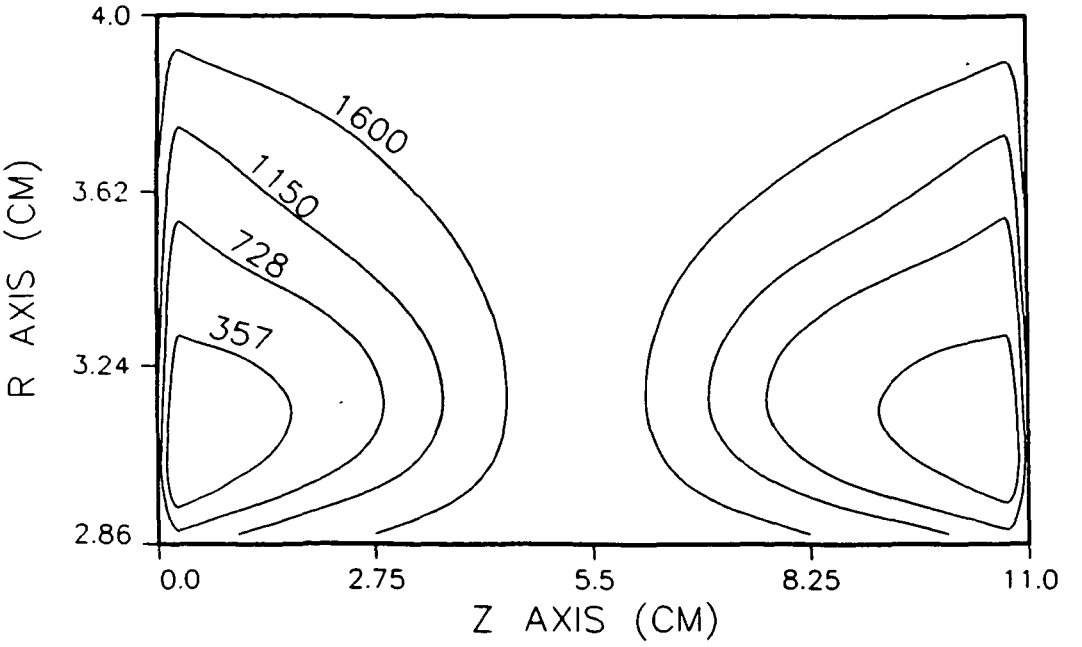

Figure 4.- Streamlines in the *zr* - plane for Trial 3
with the outer cylinder rotating at 18 rpm and the inner cylinder rotating at 36 rpm.

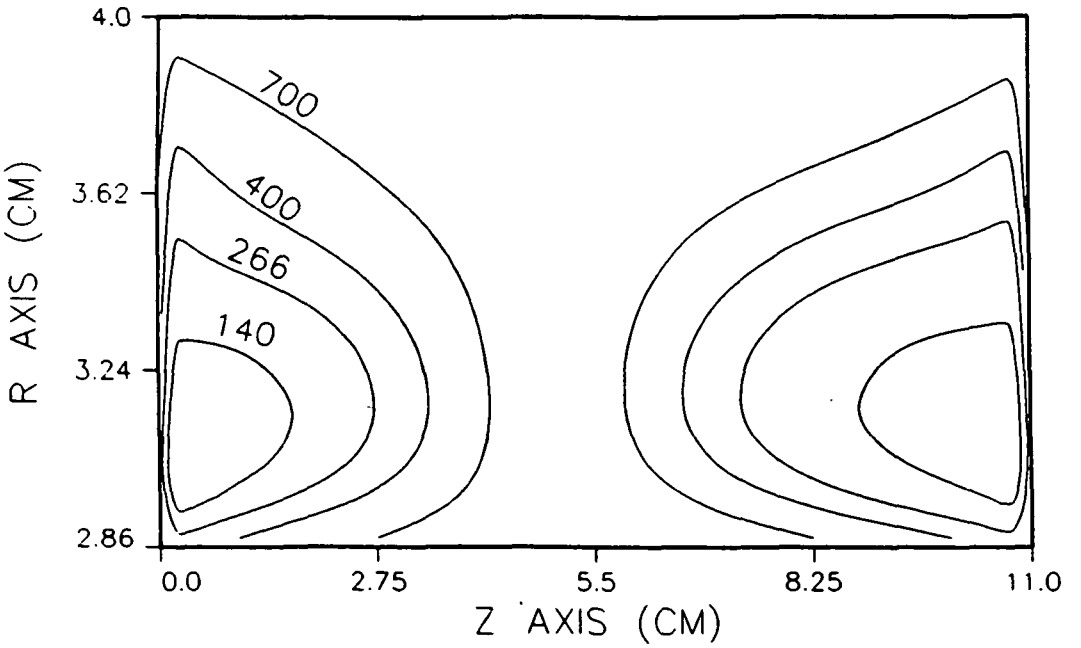

Figure 5.- Streamlines in the *zr* - plane for Trial 4
with the outer cylinder rotating at 12 rpm and the inner cylinder rotating at 36 rpm.

very slow since u and w are close to zero. These figures indicate that there may be some concern about poor circulation in the middle of the vessel. For instance, Trial 1 shows circulation time approximately equal to two hours, while increasing rpm's in Trial 4 shows circulation time decreases to approximately fifteen minutes. Higher differential rates of rotation will create a stronger secondary flow, but more studies are needed to determine what rate allows adequate time for mixing of the nutrient supply relative to the cells' metabolic requirements.

The streamlines are important for studies of mass transfer of nutrients and cellular waste products, but they do not represent the trajectories of particles as aggregates of cells and microcarrier beads. Equations 5 - 7 must be solved for the trajectories given the steady-state values of (u, v, w). This initial value problem is a two time-scale, three-dimensional, second order system of ordinary differential equations. The two time scales in this problem come from the large difference between the rate of rotation and the rate of circulation in the secondary flow. The fast time scale for the rotation of the vessel at approximately 20 rpm's is on the order of seconds, while the slow time scale for the circulation of the flow is on the order of minutes to hours as indicated above. Being a two time-scale problem, Equations 5 - 7 give a stiff system of ordinary differential equations with a 6×6 Jacobian matrix having at least two large eigenvalues and at least two small eigenvalues. Therefore, Gear's stiff method (ref. 8) was used to calculate trajectories.

In each of the four trials six trajectories are plotted in Figures 6 - 9 at unit gravity (g = 980 cm/sec^2) and in Figures 10 - 13 at microgravity (g = .0980 cm/sec^2). The initial conditions for these six trajectories are $r = 3$, $\theta = 0$, $z = 1, 2.5, 4, 7, 8.5$ and 10, respectively, with all first derivatives initially equal to zero. These figures show that a particle does not follow the streamlines precisely, but instead migrates across streamlines. If a particle is within a region of strong circulation, then it does complete its own cycle and remain suspended in the fluid. However, in most regions of the vessel a particle will not remain suspended and will hit either the wall of the outer cylinder or an end wall. Computation of a trajectory was terminated at a time when either it completed one cycle or it hit a wall of the vessel. The total lengths of time for trajectories are listed in Tables 2 - 5. In Trial 1 particles were taking more than twenty minutes to migrate to a wall of the vessel, while in Trial 4 this time frame was reduced to less than nine minutes. There is no appreciable difference in the time frames between unit gravity and microgravity. Thus higher differential rates of rotation do provide stronger circulation, but also appear to increase the frequency of interactions between the particles and the walls of the vessel. It is hypothesized that these interactions cause significant damage to the cells. Further analysis is required to quantitate the amount of damage incurred from a collision with a wall and to determine the response in a particle's trajectory afterwards.

The most noticable difference between trajectories in unit gravity and microgravity are the small, rapid oscillations in unit gravity shown in Figures 6 - 9, but lacking in Figures 10 - 13. These oscillations, which give the particles the appearance of tumbling, occur once every revolution of the flow field within the vessel and have amplitudes on the order of 0.02 cm. Figure 14 shows one example of these small deviations in the r-direction for sixty seconds. The amplitudes of these oscillations increase as r increases, since the outer cylinder is rotating slower than the inner cylinder, but are uniform in the z-direction. Intuitively, one can say that these oscillations represent a deviation in the trajectory at unit gravity from the trajectory at microgravity due to sedimentation downward in a stronger gravitational field.

The major advantage in using dynamic modeling in this study is the ability to calculate the total force on a particle as a function of time. Traditional studies have looked at fluid

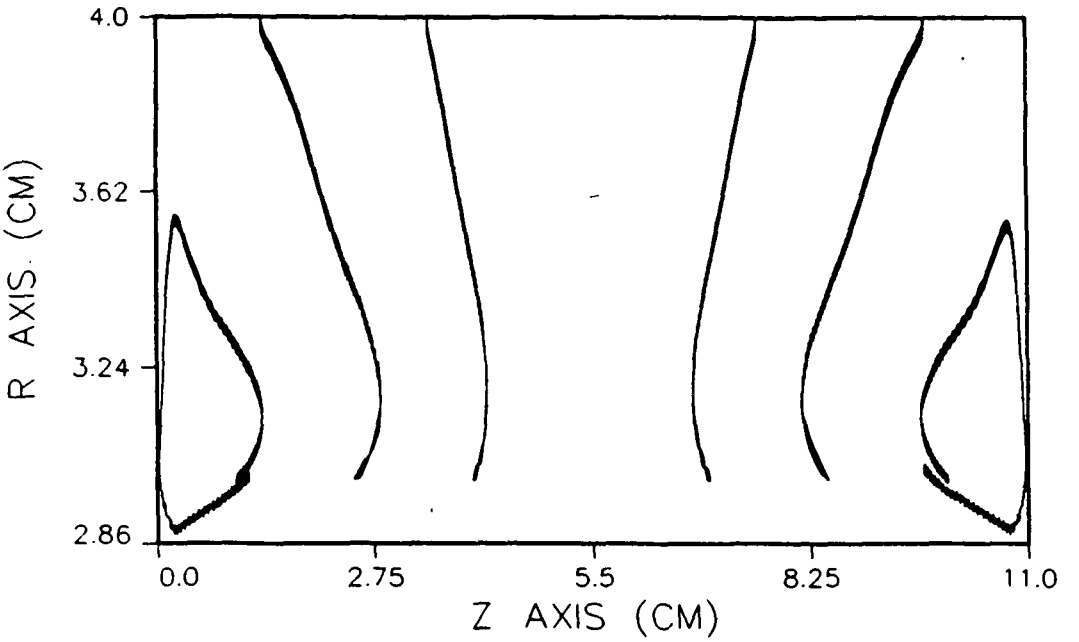

Figure 6.- Trajectories in the *zr* - plane for Trial 1
with a particle measuring 175 μm in diameter at unit gravity.

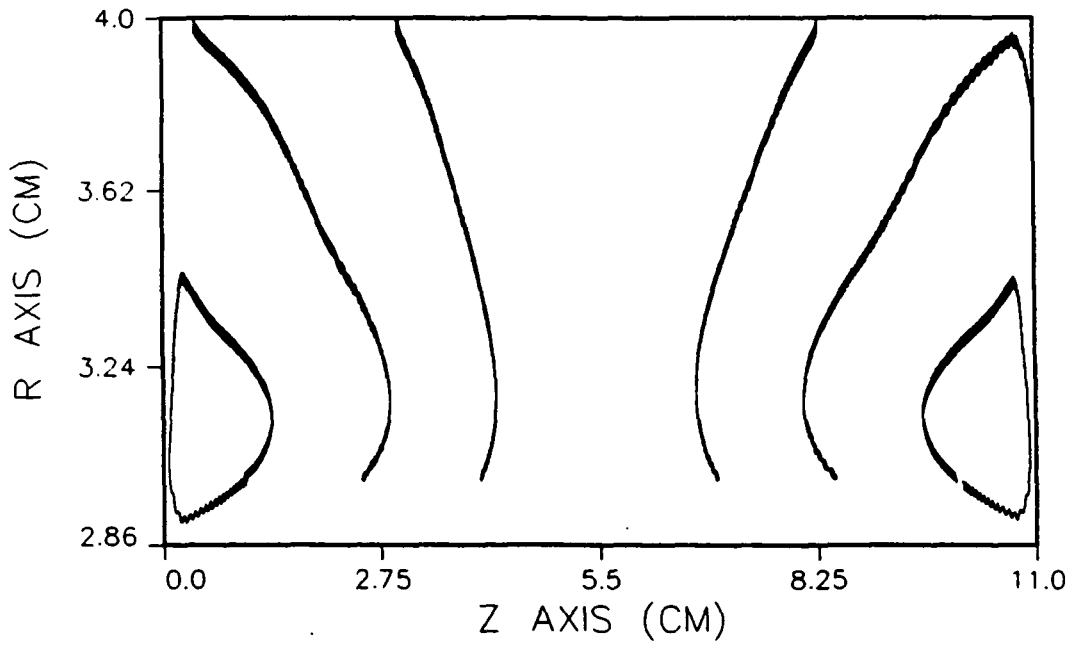

Figure 7.- Trajectories in the *zr* - plane for Trial 2
with a particle measuring 175 μm in diameter at unit gravity.

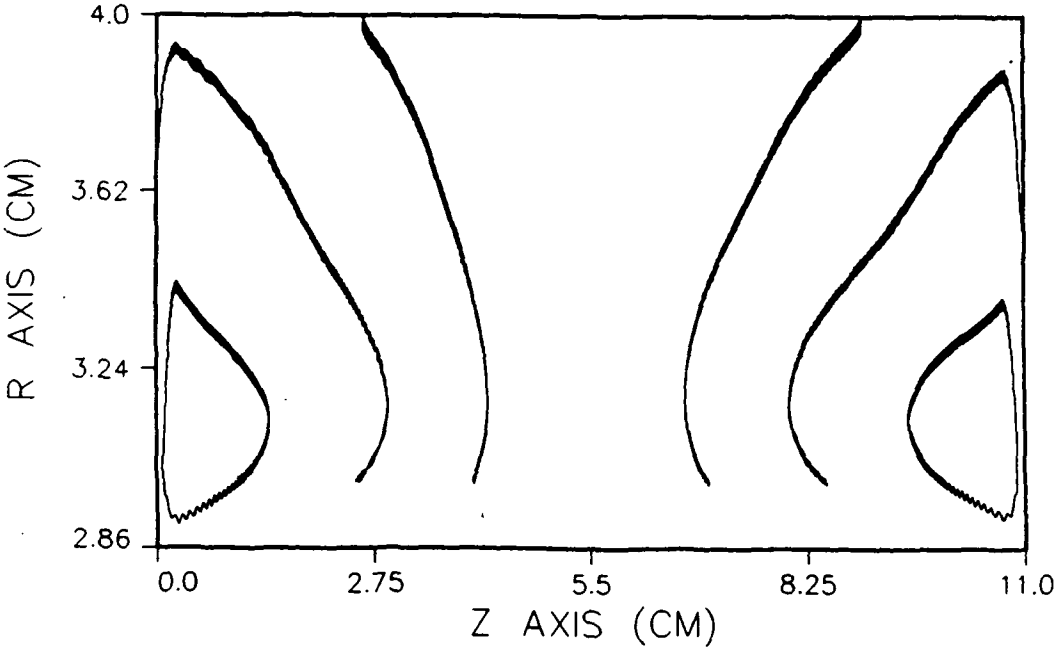

Figure 8.- Trajectories in the *zr* - plane for Trial 3
with a particle measuring 175 μm in diameter at unit gravity.

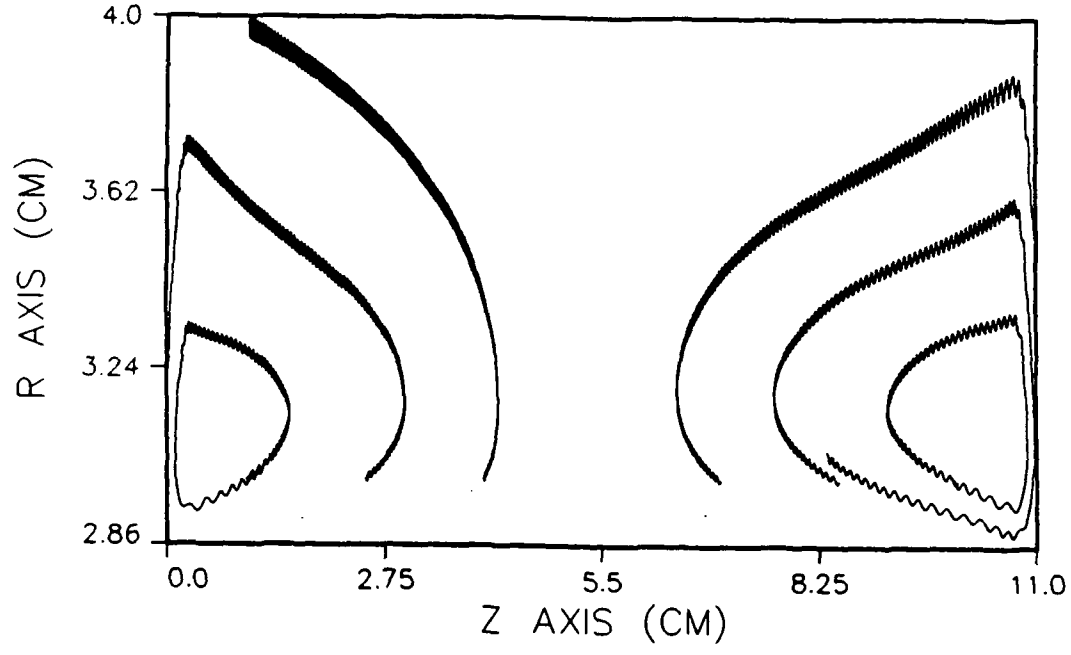

Figure 9.- Trajectories in the *zr* - plane for Trial 4
with a particle measuring 175 μm in diameter at unit gravity.

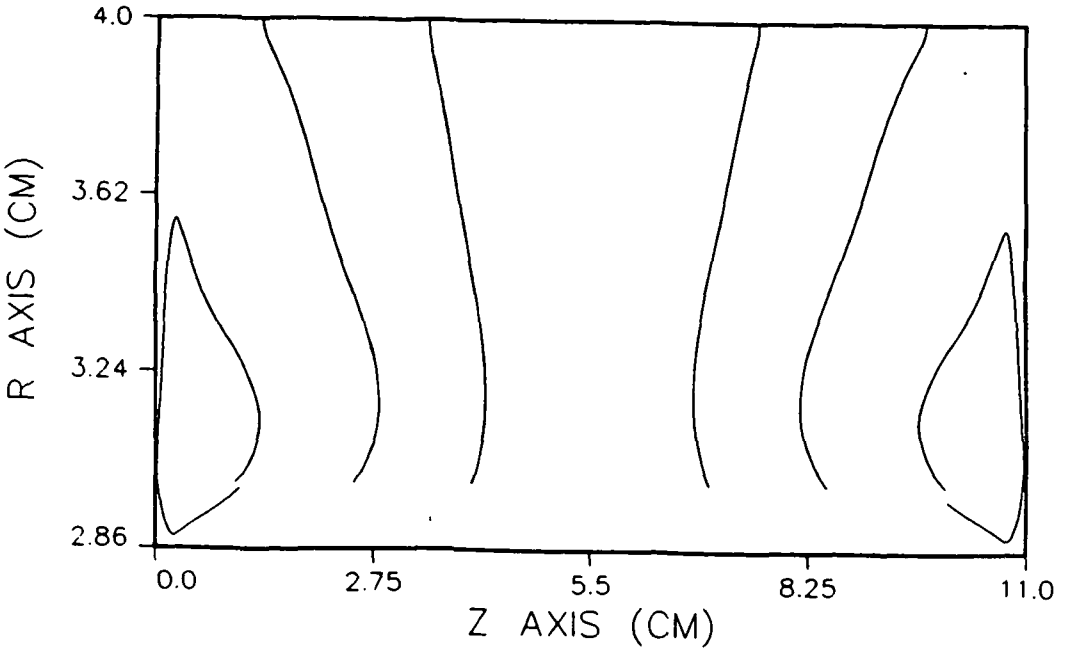

Figure 10.- Trajectories in the *zr* - plane for Trial 1
with a particle measuring 175 μm in diameter at microgravity.

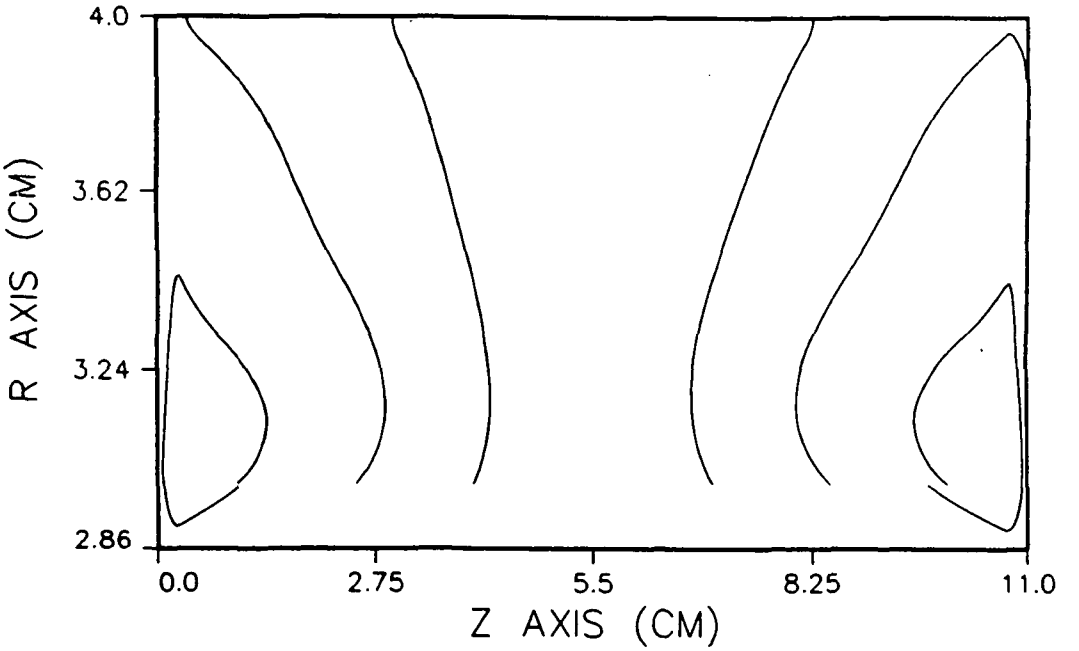

Figure 11.- Trajectories in the *zr* - plane for Trial 2
with a particle measuring 175 μm in diameter at microgravity.

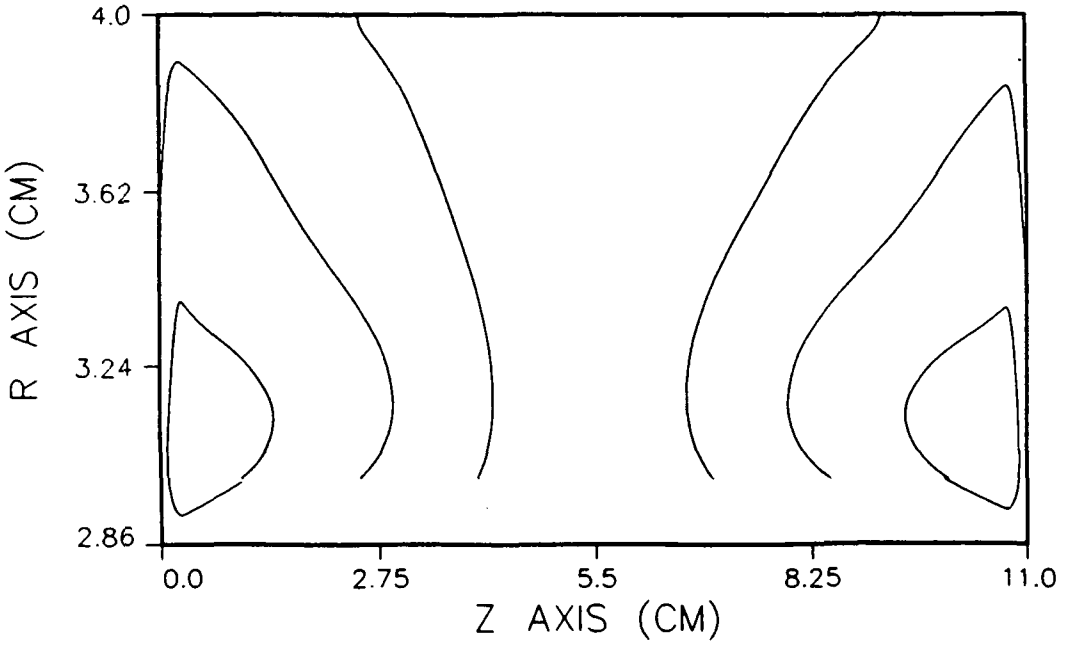

Figure 12.- Trajectories in the *zr* - plane for Trial 3
with a particle measuring 175 μm in diameter at microgravity.

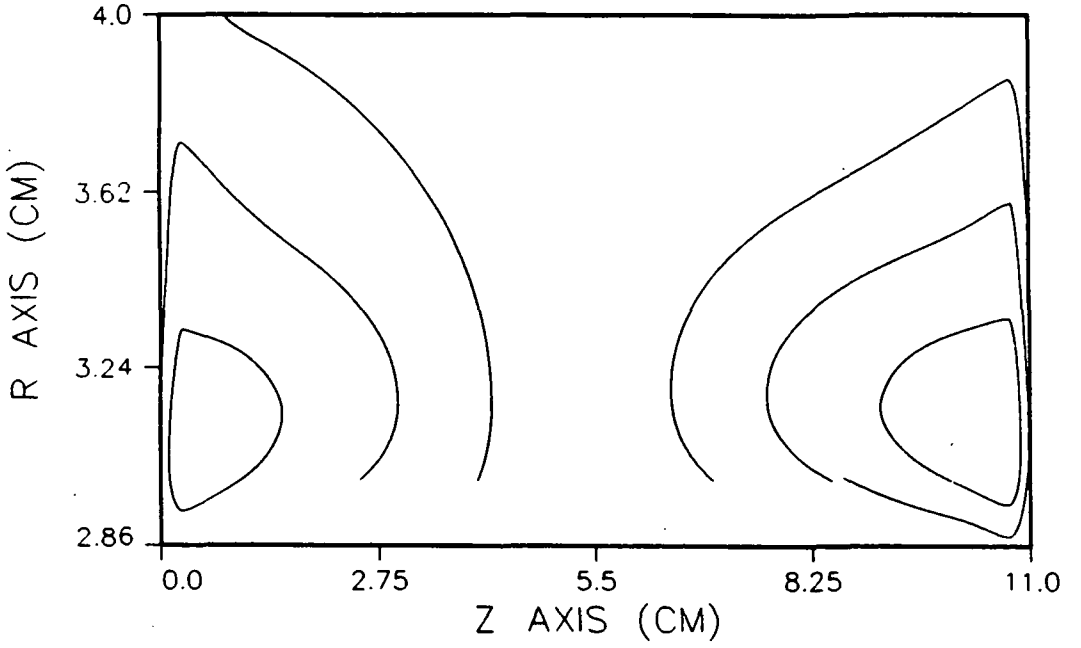

Figure 13.- Trajectories in the *zr* - plane for Trial 4
with a particle measuring 175 μm in diameter at microgravity.

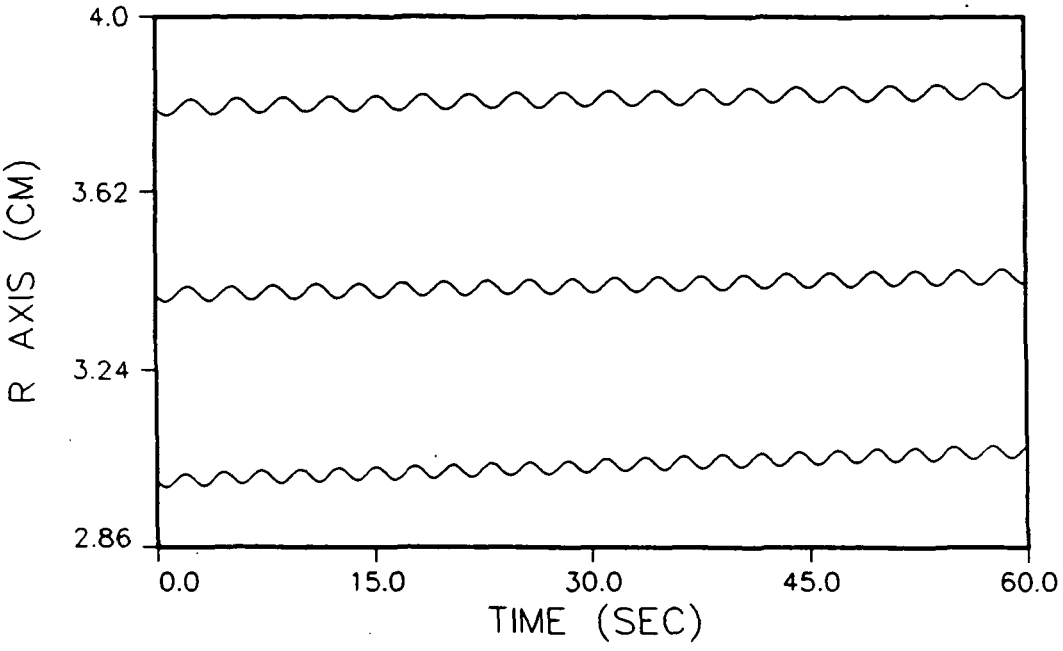

Figure 14.- Three trajectories from Trial 1
showing the r - component for sixty seconds with inital values of $\theta = 0$ and $z = 1$.

shear and drag induced by sedimentation in terms that do not reflect the dynamical response by a particle to the sum of all forces. Traditionally, from Formula 8 fluid shear relative to the cross-sectional area of a particle measured in dyne/cm^2 is given by

$$\tau = 4\mu \left| r \frac{\partial}{\partial r}\left(\frac{v}{r}\right) \right| = 8\mu r_o^2 \left| \frac{\omega_o - \omega_i}{r_o^2 - r_i^2} \right|$$

which is between 0.08 and 0.4 for the trials in this study. Drag as a force per unit cross-sectional area induced by sedimentation is

$$C_D \left[\pi \left(\frac{d}{2}\right)^2 \right] \left[\frac{1}{2} \rho_s v_\infty^2 \right]$$

where v_∞ is the terminal velocity of a particle and the drag coefficient C_D depends on the Reynolds number (ref. 9). For the trials at unit gravity in this study, drag is between 0.5 and 1.0 dyne/cm^2. The question to be answered is whether or not these values indicate the magnitude of the force on a particle in real time. In this study the total force per unit cross-sectional area on a particle can be computed in real time by calculating the vector norm of the sum of the forces in Equations 5 - 7 divided by the cross-sectional area, $\pi d^2/4$, of a particle. The maximum values and the average values over time for the total force are listed in Tables 2 - 5 for each of the six trajectories in each of the four trials at both unit gravity

and microgravity. The average force ranges from 0.0005 to 0.002 dyne/cm^2 in unit gravity and from 0.00003 to 0.0007 dyne/cm^2 in microgravity. The maximum force ranges from 0.002 to 0.013 dyne/cm^2 in unit gravity and from 0.0001 to 0.01 dyne/cm^2 in microgravity. In unit gravity drag and buoyancy seem to balance each other at approximately 0.2 - 0.4 dyne/cm^2, while centrifugal force is much smaller at approximately 0.004 - 0.007 dyne/cm^2. In microgravity the same effect is observed, but here drag and centrifugal force seem to balance each other at approximately 0.004 - 0.007 dyne/cm^2, while buoyancy is much smaller at approximately 0.00002 - 0.00004 dyne/cm^2. In general, the force on a particle in microgravity is an order of magnitude smaller than the force on a particle in unit gravity. Figures 15 and 16 show profiles in time of the force per unit cross-sectional area for sample trajectories. All of the trajectories in this study show similar profiles. Note in Figure 16 the significant increase in force experienced by the particle during the time when it is close to the end wall indicating that any damage done to the cells would most likely occur when the particle is in the neighborhood of a wall of the vessel.

TABLE 2.- RESULTS ON TRAJECTORIES IN TRIAL 1 AT 6 RPM DIFFERENTIAL.

	Unit gravity			Microgravity		
Initial Z-coord (cm)	Time (sec)	Average Force (dyne/cm^2)	Maximum Force (dyne/cm^2)	Time (sec)	Average Force (dyne/cm^2)	Maximum Force (dyne/cm^2)
1.0	1000	.0006	.0029	1000	.00005	.0003
2.5	1335	.0005	.0026	1368	.00004	.0001
4.0	1356	.0005	.0016	1389	.00004	.0003
7.0	1356	.0005	.0018	1387	.00003	.0002
8.5	1339	.0005	.0016	1371	.00004	.0003
10.0	1000	.0006	.0029	950	.00006	.0007

TABLE 3.- RESULTS ON TRAJECTORIES IN TRIAL 2 AT 12 RPM DIFFERENTIAL.

	Unit gravity			Microgravity		
Initial Z-coord (cm)	Time (sec)	Average Force (dyne/cm^2)	Maximum Force (dyne/cm^2)	Time (sec)	Average Force (dyne/cm^2)	Maximum Force (dyne/cm^2)
1.0	430	.0009	.0046	430	.00013	.0014
2.5	930	.0007	.0020	960	.00005	.0002
4.0	980	.0007	.0026	1013	.00005	.0002
7.0	977	.0007	.0029	1010	.00005	.0003
8.5	1000	.0007	.0022	1160	.00006	.0003
10.0	400	.0010	.0029	430	.00013	.0014

TABLE 4.- RESULTS ON TRAJECTORIES IN TRIAL 3 AT 18 RPM DIFFERENTIAL.

	Unit gravity			Microgravity		
Initial Z-coord (cm)	Time (sec)	Average Force (dyne/cm^2)	Maximum Force (dyne/cm^2)	Time (sec)	Average Force (dyne/cm^2)	Maximum Force (dyne/cm^2)
1.0	270	.0014	.0048	275	.00028	.0034
2.5	905	.0010	.0026	894	.00010	.0004
4.0	765	.0010	.0032	845	.00009	.0002
7.0	751	.0010	.0024	832	.00009	.0003
8.5	684	.0011	.0083	736	.00015	.0018
10.0	250	.0014	.0048	9265	.00028	.0034

TABLE 5.- RESULTS ON TRAJECTORIES IN TRIAL 4 AT 24 RPM DIFFERENTIAL.

	Unit gravity			Microgravity		
Initial Z-coord (cm)	Time (sec)	Average Force (dyne/cm^2)	Maximum Force (dyne/cm^2)	Time (sec)	Average Force (dyne/cm^2)	Maximum Force (dyne/cm^2)
1.0	125	.0021	.0107	125	.00068	.0097
2.5	337	.0016	.0053	345	.00033	.0034
4.0	541	.0014	.0036	604	.00015	.0005
7.0	432	.0016	.0063	600	.00031	.0021
8.5	265	.0019	.0132	265	.00055	.0115
10.0	125	.0021	.0125	125	.00066	.0099

In conclusion, the rotating bioreactors being developed by the biotechnology group at NASA Johnson Space Center do partially simulate microgravity with respect to the trajectories and time frame of a particle's motion. However, there is still a distinct advantage to having the bioreactor in microgravity since the total force on a particle would be significantly reduced. The total force on a particle in a rotating bioreactor is less than one might anticipate from the values reported by other researchers using different geometries to model hydrodynamic effects on cell growth. In either unit gravity or microgravity it appears that the greatest potential for damage to the cells comes when the particle is near to a wall of the vessel or actually collides with a wall. Hence, further study needs to be conducted to determine an optimal design and optimal rates of rotation to minimize the migration of particles toward the outside cylinder and still provide adequate circulation for sufficient mass transfer of nutrients and cellular waste products.

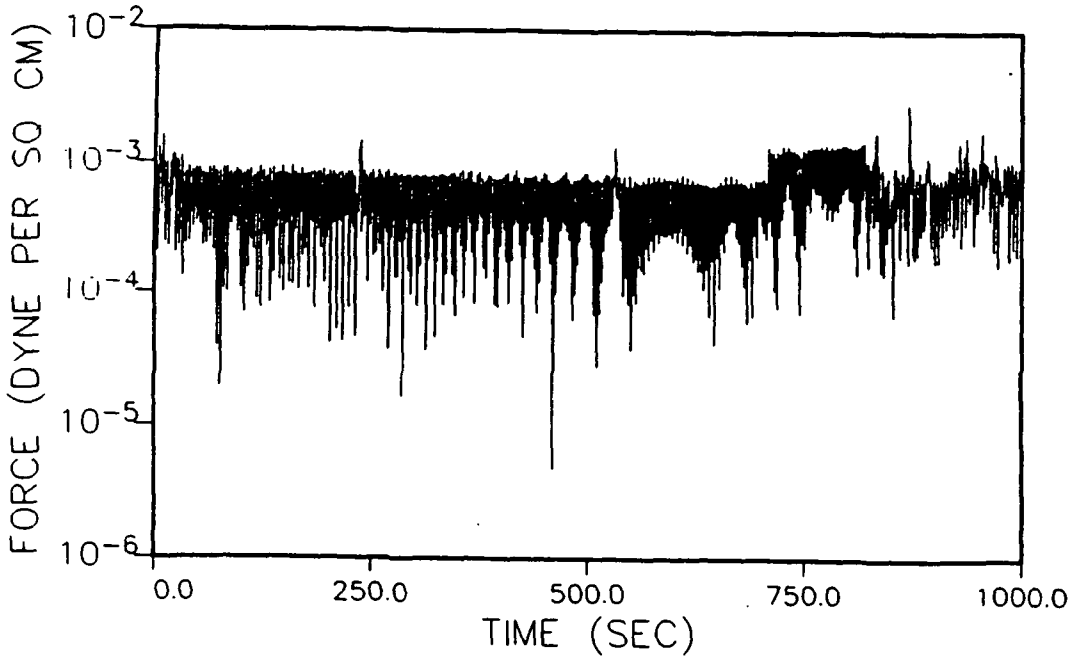

Figure 15.- Force per unit area on a particle
for the trajectory starting at $r = 3$, $\theta = 0$ and $z = 1$ in Trial 1 at unit gravity.

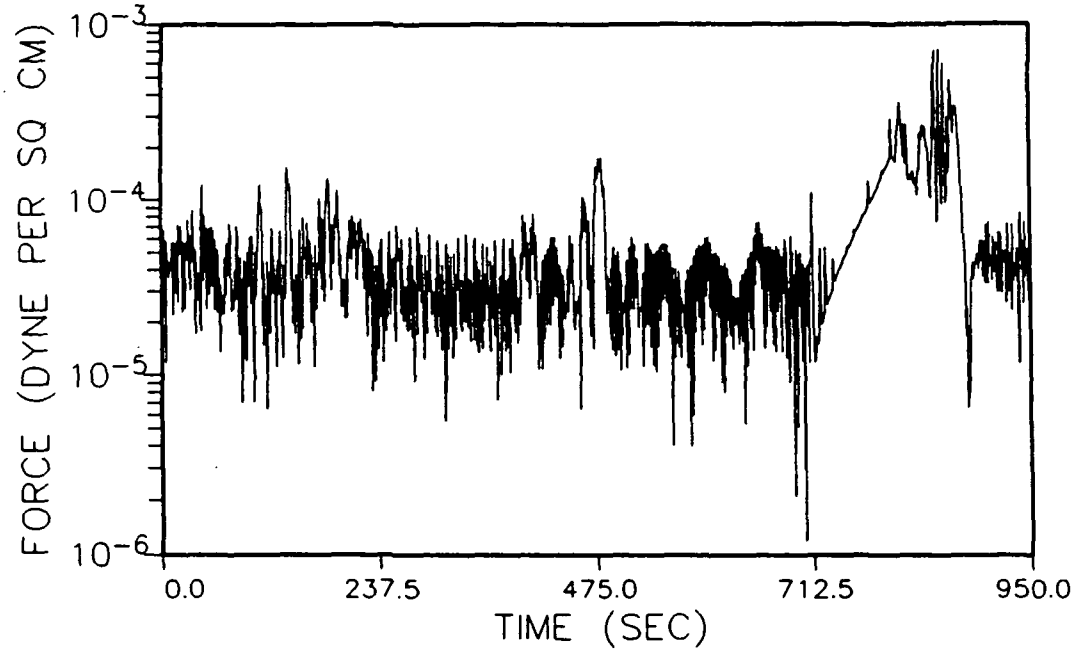

Figure 16.- Force per unit area on a particle
for the trajectory starting at $r = 3$, $\theta = 0$ and $z = 10$ in Trial 1 at microgravity.

REFERENCES

1. Cherry, R. S.; and Papoutsakis, E. T.: Hydrodynamic Effects on Cells in Agitated Tissue Culture Reactors. *Bioprocess Engineering*, vol. 1, 1986, pp. 29 - 41.

2. Cherry, R. S.; and Papoutsakis, E. T.: Physical Mechanisms of Cell Damage in Microcarrier Cell Culture Bioreactors. *Biotechnology and Bioengineering*, vol. 32, 1988, pp. 1001 - 1014.

3. Croughan, M. S.; Hamel, J. F.; and Wang, D. I. C.: Hydrodynamic Effects on Animal Cells Grown in Microcarrier Cultures. *Biotechnology and Bioengineering*, vol. 29, 1987, pp. 130 - 141.

4. Croughan, M. S.; and Wang, D. I. C.: Growth and Death in Overagitated Microcarrier Cell Cultures. *Biotechnology and Bioengineering*, vol. 33, 1989, pp. 731 - 744.

5. Patankar, S. V.: *Numericla Heat Transfer and Fluid Flow*. McGraw-Hill, New York, 1980, p. 197.

6. Schlichting, Hermann: *Boundary-Layer Theory*. McGraw-Hill, New York, 1979, p. 87.

7. Burden, R. L.; and Faires, J. D.: *Numerical Analysis*. PWS-Kent, Boston, 1989, pp. 251 - 255.

8. Burden, R. L.; and Faires, J. D.: *Numerical Analysis*. PWS-Kent, Boston, 1989, pp. 302 - 308.

9. Bird, R. B.; Stewart, W. E.; and Lightfoot, E. N.: *Transport Phenomena*, John Wiley and Sons, New York, 1960, pp. 190 - 194.